Guanidine-Induced Equilibrium Unfolding of a Homo-Hexameric Enzyme 4-Oxalocrotonate Tautomerase (4-OT)†

Peter Silinski, Michael J. Allingham, and Michael C. Fitzgerald*

Department of Chemistry, Duke University, Durham, North Carolina, 27708

Received December 4, 2000; Revised Manuscript Received February 8, 2001

ABSTRACT: 4-Oxalocrotonate tautomerase (4-OT) is a bacterial enzyme that is comprised of 6 identical 62 amino acid subunits. The 4-OT enzyme is an attractive model system in which to study the interrelationship between protein folding, subunit assembly, and catalytic function. Here we report on the GuHCl-induced equilibrium unfolding properties of wild-type 4-OT using catalytic activity measurements and using far-UV circular dichroism (CD) spectroscopy. We demonstrate that the unfolding of wild-type 4-OT in 50 mM phosphate buffers containing 6 M GuHCl is reversible at pHs 6.0, 7.4, and 8.5; and we find that there is both an enzyme concentration dependence and a pH dependence to the equilibrium unfolding properties of 4-OT. Our data suggests that the GuHCl-induced unfolding of 4-OT in 50 mM phosphate buffer at pH 8.5 can be modeled as a two-state process involving folded hexamer and unfolded monomer. On the basis of this model, we determined a free-energy value for the unfolding of 4-OT at pH 8.5 to be 68.7 ± 3.2 kcal/mol under standard state conditions (1 M hexamer). In 50 mM phosphate buffers at pHs 6.0 and 7.4, only the catalytic activity denaturation curves are consistent with a two-state folding mechanism. At the lower pHs the far-UV-CD transitions are not well described by a two-state model. Our results at pHs 6.0 and 7.4 suggest that intermediate state(s) are populated in the equilibrium unfolding reaction at these lower pHs and that these intermediate state(s) have some helical content but no measurable catalytic activity.

Oligomeric proteins play important roles in a number of cellular processes from metabolism to transcription. However, relatively little is known about the detailed mechanisms by which multimeric proteins acquire their higher order structure in vivo or in vitro. Much of what is currently known about protein folding and stability has been gleaned from theoretical and experimental investigations on small, monomeric proteins and protein domains ranging from 50 to 150 amino acids in size. Studies on a number of model, monomeric protein systems have helped elucidate many important factors in protein folding reactions. For example, it is has been established that electrostatic interactions (*1*), hydrogen bonding (*2*−*4*), the hydrophobic effect (*1*), folding nuclei (*5*), and partially folded intermediates (*6*) can play important roles in the process by which a single polypeptide chain acquires its secondary and tertiary structure. Much less is known about the contribution of these factors to quaternary structure formation in protein folding reactions.

Biophysical studies on several dimeric protein systems have provided some insight into the folding and assembly reactions of oligomeric proteins. The dimeric P22 Arc repressor has been observed in both equilibrium and kinetic studies to fold according to a strictly two-state (folded and unfolded) mechanism (*7*). Equilibrium unfolding studies on the dimeric *Escherichia coli Trp* repressor and on the dimeric dihydrofolate reductase from the hyperthermophilic bacterium *thermotoga maritima* also revealed two-state folding behavior. However, transient, partially folded intermediates have been detected in kinetic studies on the folding reactions of these two proteins (*8*−*10*). Equilibrium experiments with the dimeric α-subunit of bacterial luciferase and the tertrameric lactose repressor protein have also revealed multistate unfolding mechanisms for these protein systems (*11*, *12*). The folding pathways of several higher order multimeric protein systems including the trimeric tail spike protein, the tetrameric lactate dehydrogenase, and the hexameric UDP glucose dehydrogenase have also been examined, and it appears that the folding reactions of these large protein complexes proceed through complex pathways involving multiple folding intermediates (*13*). Unfortunately, the complexity of the folding mechanisms for these multisubunit proteins has limited the amount of detailed information that can be extracted from biophysical studies of their folding and assembly.

Here we describe initial biophysical studies on a new model, oligomeric protein system 4-oxalocrotonate tautomerase (4-OT).[1] 4-OT is a 41 kDa bacterial enzyme that consists of six identical 62-amino acid subunits (*14*, *15*). The enzyme functions as part of a catechol meta-fission pathway in certain soil bacteria, where it is responsible for the ketonization of 2-hydroxymuconate (2-HM) to the corresponding α,β-unsaturated ketone, 2-oxo-3-hexenedioate (*16*). The catalytic properties of 4-OT have been well studied over the past decade (*16*−*23*). There is significant biochemical evidence indicating that Pro-1 is the general base catalyst

† This work was supported by Duke University and the Research Corporation. P.S. was supported by funds from an NIH sponsored Biological Training Program at Duke University.

* To whom correspondence should be addressed. Phone: (919) 660-1547. Fax: (919) 660-1605. E-mail: mfitz@chem.duke.edu.

10.1021/bi002752b CCC: $20.00
Published on Web 03/15/2001

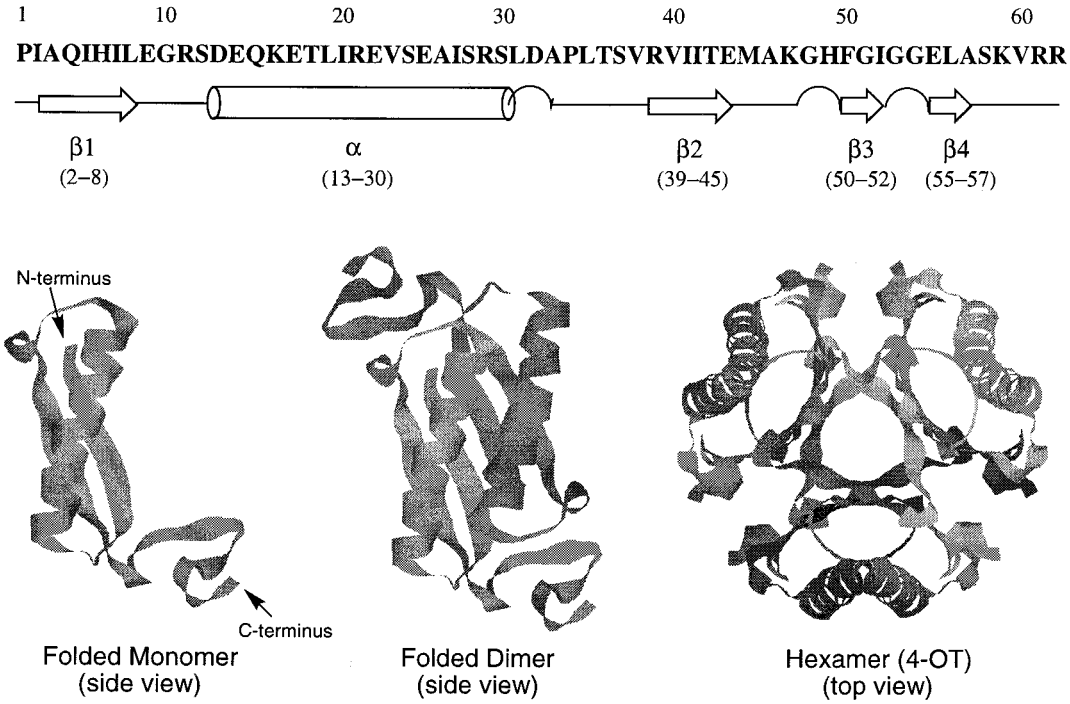

FIGURE 1: Schematic representation of 4-OT's primary, secondary, and tertiary structure.

and the enzyme appears to operate in a suprafacial process consistent with a single base mechanism (*20*, *21*). Two arginine residues (Arg-11, Arg-39) from two adjacent subunits of the enzyme have also been implicated in substrate binding (*15*, *23*).

While many of the catalytic properties of 4-OT have been elucidated, the enzyme is a new model system for protein folding studies. Recently, a qualitative analysis of backbone-backbone hydrogen bonds involving the peptide bond between Pro-1 and Ile-2 demonstrated the importance of these noncovalent interactions in the folding specifity of 4-OT (*24*). However, nothing is known about the equilibrium or kinetic properties of 4-OT's unfolding or refolding reaction. The 4-OT molecule is an especially attractive model system in which to study the relationship between folding and assembly because its folded structure is defined completely by noncovalent interactions. There are no disulfide bonds between or within subunits. Moreover, this highly efficient enzyme system, with catalytic rates approaching diffusion controlled limits, provides a unique opportunity to study the interrelationships between protein folding, subunit assembly, and enzyme function.

The three-dimensional structure of 4-OT has been solved by X-ray crystallographic methods, and the enzyme complex resembles a trimer of dimers (see Figure 1) (*15*, *25*). It has been noted that 4-OT shares a newly discovered $\beta-\alpha-\beta$ structural motif with two other proteins including another bacterial enzyme, 5-carboxymethyl-2-hydroxymuconate isomerase (CHMI), and a chemokine, macrophage migration inhibitory factor (MIF) (*26*). This is despite differences in the stoichiometry of their subunits and significant differences in their primary amino acid sequences. While 4-OT is a hexameric enzyme of 6 identical 62-amino acid subunits, CHMI and MIF are trimeric enzymes of 3 identical 125- and 114-amino acid subunits, respectively. A 4-OT dimer is structurally equivalent to a MIF and CHMI monomer. The structural similarities between a 4-OT dimer and monomer units in CHMI and MIF along with the orientation of 4-OT's catalytic residues within a dimer unit raise interesting questions about the relative stability and catalytic competence of a 4-OT dimer. One goal of this study was to determine if such a dimeric structure is populated under equilibrium conditions.

Here we report on the GuHCl-induced equilibrium unfolding properties of wild-type 4-OT using catalytic activity measurements with the substrate, 2-hydroxymuconate (2-HM) and far-UV circular dichroism (CD) spectroscopy as structural probes. We demonstrate that the unfolding of the enzyme in 50 mM phosphate buffers containing 6 M GuHCl is reversible at pHs 6.0, 7.4, and 8.5; and we find that there is both a protein concentration dependence and a pH dependence to the equilibrium unfolding behavior of 4-OT. Our data at pH 8.5 suggest that the GuHCl-induced unfolding of 4-OT at this pH can be modeled as a two-state process involving only folded hexamer and unfolded monomer. However, in phosphate buffers at pH 7.4 and 6.0, only the catalytic activity transition is well described by a two-state model. The far-UV-CD transitions at these lower pHs are not consistent with a two-state folding mechanism. Our results suggest that intermediate state(s) appear to be populated at these lower pHs. These intermediate state(s) appear to be more significantly populated at pH 6.0 than at pH 7.4. Moreover, our data are not consistent with the

[1] Abbreviations: 4-OT, 4-oxalocrotonate tautomerase; 2-HM, 2-hydroxymuconate; GuHCl, guanidine hydrochloride; PMSF, phenylmethanesulfonyl fluoride; IPTG, isopropyl-β,D-thiogalactopyranoside; TFA, trifluoroacetic acid; UV-CD, ultraviolet circular dichroism; LB, Luria-Bertani medium; RP-HPLC, reversed-phase high-performance liquid chromatography; ESI-MS, electrospray ionization mass spectrometry; F_{app}, apparent fraction of unfolded enzyme; $[P_{tot}]_M$, total protein concentration in terms of monomer; ΔG_{app}, apparent free-energy change of unfolding; ΔG_{H_2O}, free-energy change of unfolding in the absence of denaturant.

formation of catalytically competent 4-OT dimers under equilibrium conditions.

MATERIALS AND METHODS

Materials. Sodium dihydrogenphosphate, disodium hydrogenphosphate, and phenylmethanesulfonyl fluoride (PMSF) were purchased from Sigma. The GuHCl was obtained from OmniPur. Peptone, agar, and yeast extract were obtained from Mikrobiologie. Kanamycin was obtained from Shelton Scientific, and isopropyl-β,D-thiogalactopyranoside (IPTG) was obtained from Life Technologies. Competent *Epicurian Coli* BL21-Gold(DE3) cells were obtained from Stratagene. HPLC grade acetonitrile was obtained from Mallinckrodt and neat trifluoroacetic acid (TFA) was purchased from Halocarbon. 2-HM was a gift from Professor Christian P. Whitman (University of Texas at Austin). All other chemicals were of reagent grade or better.

General Methods and Instrumentation. Analytical and preparative reversed-phase high-perfomance liquid chromatography (RP-HPLC) were performed on a Rainin instrument that included a Dynamax SD-200 Solvent Delivery System and a Dynamax variable wavelength UV−vis absorbance detector. Analytical RP-HPLC was performed on a C_{18} Vydac column (0.46 × 15.0 cm, 300 Å) at a flow rate of 1 mL/min. Preparative RP-HPLC separations were performed using a C_{18} Vydac column (2.2 × 25.0 cm, 300 Å) at a flow rate of 10 mL/min. Analytical and preparative RP-HPLC separations were performed using linear gradients of buffer B in A (buffer A = 0.1% TFA in water, buffer B = 90% acetonitrile in water containing 0.09% TFA). Detection was at 214 nm for analytical separations and at 230 nm for preparative separations. Mass spectra were obtained using a PE-Sciex API 150EX electrospray mass spectrometer. For mass spectral analyses protein samples were typically diluted into a buffer containing 40% buffer B and 60% buffer A and then infused directly into the mass spectrometer at a flow rate of 10 μL/min using a Harvard Syringe pump. All UV−vis absorbance data was collected using a Hewlett-Packard 8452A Diode Array UV−vis Spectrophotometer. All far-UV-CD measurements were performed on a Jasco J-710 Spectropolarimeter using a bandwidth of 1.0 nm.

Protein Expression and Purification. A pET24a plasmid containing the wild-type 4-OT gene within the *Sal*I and *Nde*I restriction sites was kindly provided by Professor Christian P. Whitman (University of Texas at Austin). The plasmid vector was transformed into competent *Epicurian Coli* BL21-Gold(DE3) cells by heat shock at 42 °C, and the cells were grown on LB/kanamycin (50 μg/mL) plates at 37 °C. Individual colonies were harvested overnight in 5 mL of LB/kanamycin, then grown to log phase in 1 L of LB/kanamycin while shaking at 37 °C. Protein expression was induced by the addition 250 mg/L IPTG, and the cells were allowed to grow for an additional 4 h. The cells were pelleted by centrifugation, resuspended in 50 mM phosphate buffer (pH 7.4) containing 2 mM PMSF, and lysed by sonication. Cell debris was removed by centrifugation, and the desired product were purified from the crude cell lysate by preparative RP-HPLC using a 40 to 60% linear gradient of buffer B in A. Pure RP-HPLC fractions of 4-OT, as judged by ESI-MS analysis, were combined, frozen, and lyophilized to a dry, white powder.

Equilibrium Studies: Experimental Conditions. All equilibrium experiments in this work were carried out at 25 °C in 50 mM phosphate buffers (pH 6.0 7.4, or 8.5) containing varying amounts of GuHCl. GuHCl concentrations were determined by refractive index measurements at 25 °C (*27*). Enzyme concentrations were determined in terms of monomer using the Waddell method (*28*).

In experiments to evaluate the reversibility of the wild-type 4-OT unfolding reaction, stock solutions of the folded and the unfolded enzyme were each prepared from a single concentrated solution of the enzyme in 50 mM phosphate buffer containing 6 M GuHCl. The folded enzyme stock solution was prepared by a 38-fold dilution of this concentrated, GuHCl denatured 4-OT solution with 50 mM phosphate buffer (pH 7.4). The unfolded enzyme stock solution was prepared by a 38-fold dilution of the concentrated, GuHCl denatured 4-OT solution with 50 mM phosphate buffer (pH 7.4) containing 6 M GuHCl. Catalytic activity and far-UV-CD measurements on the resulting solutions confirmed that the enzyme in the folded stock solutions displayed nativelike properties and that the enzyme in the unfolded stock solution was in a nonnative, denatured state. The protein solutions used to generate the 4-OT unfolding curve were prepared by dilution (≥10-fold) of the folded enzyme stock solution into a series of 50 mM buffer solutions (pH 7.4) containing different amounts of GuHCl. The protein solutions used to generate the 4-OT refolding curve were prepared by dilution (≥10-fold) of the unfolded enzyme stock solution into a series of 50 mM buffer solutions (pH 7.4) containing different amounts of GuHCl. The final concentration of 4-OT in these unfolding and refolding experiments was 8 μM (based on monomer) and GuHCl concentrations ranged from 0.1 to 6 M.

After it was established that the 4-OT unfolding reaction was reversible, the protein solutions used to generate subsequent GuHCl-induced equilibrium unfolding curves in this work were prepared by mixing two different stock solutions of the enzyme. One stock solution contained the folded enzyme in 50 mM phosphate buffer, and the other stock solution contained the unfolded enzyme in 50 mM phosphate buffer with 6 M GuHCl. Both of these stock solutions were prepared by dilution (always ≥10-fold) of the same concentrated, 6 M GuHCl denatured 4-OT solution. The folded and unfolded stock solutions of 4-OT were mixed in appropriate ratios to generate a series of equimolar protein solutions with GuHCl concentrations that varied from 0.1 to 6.0 M. After mixing, the pH of each solution was adjusted to within ±0.1 pH units of the desired pH by the addition of small volumes (less than 1% v/v) of 1 N NaOH. All solutions were allowed to equilibrate at room temperature for at least 20 h before analysis. Each solution was also visually inspected to confirm that no precipitate had formed.

4-OT's catalytic activity was assayed using the substrate 2-HM. Catalytic rates were determined by monitoring the rate of product formation. This was accomplished by monitoring the change in absorbance at 232 nm in 1-s intervals over a 5-s time period, and then performing linear least-squares analysis in order to obtain the rate in AU/s. All activity measurements were recorded before the enzyme had a chance to refold during the necessary dilutions of the assay. Data were collected in triplicate for each enzyme solution.

CD denaturation curves at each pH and at each enzyme concentration were recorded by monitoring the far-UV-CD signal at 222 nm and at 25 °C. Far-UV-CD data was collected by averaging the signal at 0.5-s intervals for 30 s. Far-UV-CD measurements were obtained using a 0.5 cm quartz cuvette for 4-OT solutions >70 μM and using a 1 cm quartz cuvette for the less concentrated protein solutions. Far-UV-CD and catalytic activity measurements were obtained from the same set of solutions at each enzyme concentration and at each pH that was studied.

Equilibrium Studies: Data Analysis. Raw data from far-UV-CD and catalytic rate measurements were normalized by converting the raw signal to an apparent fraction of unfolded enzyme (F_{app}) according to eq 1 (*29*):

$$F_{app} = \frac{S - S_F}{S_F - S_U} \quad (1)$$

where S is the far-UV-CD signal at 222 nm or the catalytic rate measured when the enzyme was equilibrated at a given GuHCl concentration, and S_F and S_U are the respective signals of the folded and unfolded forms of the enzyme at each GuHCl concentration. In our experiments, S was linearly dependent on the GuHCl concentration in both the folded and unfolded baseline regions for both of the structural probes used in this study (i.e., CD and catalytic activity). Therefore, linear extrapolations from these baselines were used to estimate S_F and S_U values in the transition region.

Normalized data were fit to the following two-state (folded and unfolded) model:

$$H \leftrightarrow 6M \quad (2)$$

where H represents folded 4-OT hexamer and M represents unfolded monomer. The equilibrium constant for the unfolding reaction in eq 2 can be written in the following form:

$$K_{eq} = \frac{6[M]^6}{[P_{tot}]_M - [M]} \quad (3)$$

where $[P_{tot}]_M$ is the total protein concentration in terms of monomer and [M] is the concentration of unfolded monomer. If the apparent fraction of unfolded enzyme, $F_{app,}$ is defined as $[M]/[P_{tot}]_M$, the equilibrium constant in eq 3 can be rewritten in the following form:

$$K_{app} = \frac{6F_{app}{}^6[P_{tot}]_M{}^5}{1 - F_{app}} \quad (4)$$

where K_{app} is the apparent equilibrium constant at each GuHCl concentration. For a two-state unfolding process and at moderate to high denaturant concentrations the apparent free energy of unfolding (ΔG_{app}) is linearly dependent on the molar concentration of the denaturant according to eq 5 (*29*, *30*):

$$\Delta G_{app} = \Delta G_{H_2O} + m_g[\text{denaturant}] \quad (5)$$

where ΔG_{app} is the apparent free energy of unfolding at a particular denaturant concentration at standard state (1 M hexamer), m_g is the constant of proportionality ($\delta\Delta G_{app}/\delta$-[denaturant]), and ΔG_{H_2O} is the free-energy change of unfolding in the absence of denaturant.

In equilibrium studies of the chemical denaturant-induced unfolding of proteins, thermodynamic parameters are typically obtained by using a nonlinear least-squares analysis to fit the dependence of F_{app} upon the chemical denaturant concentration. This global fitting of the data requires an expression for F_{app} in terms of [denaturant], $[P_{tot}]_M$, ΔG_{H_2O}, and m_g. Such an expression can be derived from eqs 4 and 5; however, due to the high order of eq 4 there is not a unique solution. This ultimately precludes the use of standard nonlinear least-squares analysis programs based on the Marquardt−Levenberg algorithm to fit the data in our denaturation curves (*31*). Therefore, in our two-state analyses of the equilibrium unfolding curves in this work we extracted ΔG_{H_2O} and m_g values from the data by using eq 4 and the expression $\Delta G_{app} = -RT \ln(K_{app})$ to convert F_{app} values in the transition region of each denaturation curve to ΔG_{app} values. These ΔG_{app} values were then used to generate ΔG_{app} vs [GuHCl] plots. A linear least-squares analysis of these plots yielded an m_g value and an extrapolated ΔG_{H_2O} value.

RESULTS

Reversible Denaturation of Wild-Type 4-OT. Wild-type 4-OT was reversibly denatured in 50 mM phosphate buffer containing 6 M GuHCl at protein concentrations between 1 and 100 μM and at pHs between 6.0 and 8.5. Refolding yields in this protein concentration range and in this pH range were nearly 100% as judged by CD and catalytic activity measurements. We further investigated the reversibility of the GuHCl-induced equilibrium unfolding of wild-type 4-OT by examining the coincidence of unfolding and refolding curves generated using both far-UV-CD and catalytic activity measurements. The helical content of 4-OT's polypeptide chain in its native state is approximately 25%; therefore, the presence of such secondary structure is readily determined using far-UV-CD spectroscopy by measuring the enzyme's molar ellipticity at 222 nm (*32*). The enzyme's catalytic activity is readily determined in a UV spectrophotometric assay using 2-HM as the substrate (*16*). The enzyme is highly efficient; therefore, it can be assayed for catalytic activity using pmol amounts of enzyme and using reactions times less than 5 s. Thus, it is possible to assay the enzyme's activity in various states of its chemical denaturation without significant renaturation occurring in the assay. This was confirmed in a control experiment with enzyme that was denatured in 6 M GuHCl. A 5 μL aliquot of a concentrated GuHCl denatured, enzyme solution (5 mg/mL) was diluted 200-fold directly into the assay mixture. No catalytic activity was detected in the 5 s assay of this denatured enzyme.

The unfolding and refolding curves generated by monitoring the CD signal at 222 nm as a function of [GuHCl] under similar solution conditions (i.e., 50 mM phosphate buffer, pH 7.4, containing 8 μM enzyme, 25 °C) were coincident (Figure 2A). Both the unfolding and the refolding curves in this CD experiment showed a single, cooperative transition with a midpoint at approximately 1.8 M GuHCl. The same solutions used to generate the unfolding and refolding CD curves in Figure 2A were also used to confirm that the 4-OT unfolding reaction was reversible in terms of function. The catalytic activity of each solution was recorded and these data was used to generate the unfolding and refolding curves in Figure 2B. Both of these curves were also coincident and displayed a single cooperative transition

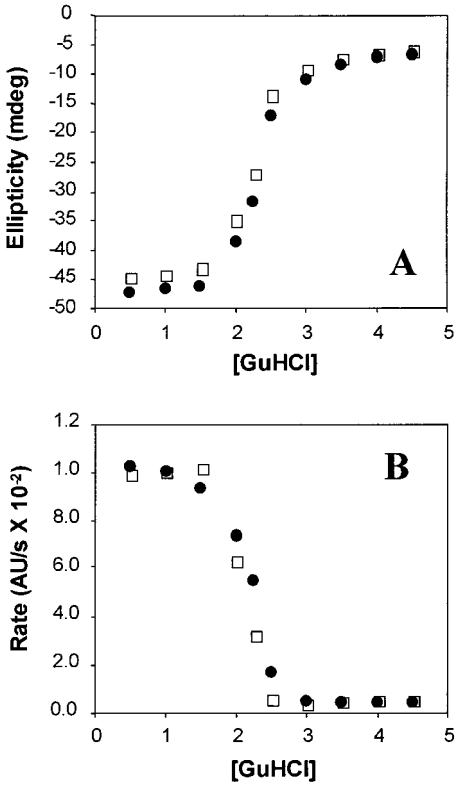

FIGURE 2: GuHCl-induced denaturation curves (closed circles) and renaturation curves (open squares) for wild-type 4-OT monitored by (A) far-UV-CD spectroscopy and by (B) catalytic activity measurements. Both the unfolding data and the refolding data were obtained with 8 μM protein solutions in 50 mM phosphate buffer (pH 7.4) at 25 °C.

with a midpoint at 1.8 M GuHCl (Figure 2B).

GuHCl-Induced Equilibrium Unfolding of Wild-Type 4-OT: pH Dependence. The GuHCl-induced equilibrium unfolding transition of wild-type 4-OT in 50 mM phosphate buffer was monitored at pH 6.0, 7.4, and 8.5 by far-UV-CD spectroscopy and by the enzyme's catalytic activity. At each pH, the raw CD and catalytic activity data were normalized to F_{app} (see Material and Methods for details) and plotted as a function of denaturant concentration (Figure 3). The data in Figure 3 was collected on solutions in which the total protein concentration, based on monomer, was 10 μM. At pH 8.5, the denaturation curves generated from the far-UV-CD data and the catalytic activity data were essentially identical (Figure 3A). Both denaturation curves displayed a single, steep unfolding transition with a midpoint of 2.5 M GuHCl. The far-UV-CD and catalytic activity denaturation curves recorded at pH 7.4 were similar to those recorded at pH 8.5 (Figure 3B). However, it is noteworthy that the transition midpoints for the far-UV-CD and catalytic activity curves at pH 7.4 are not exactly coincident. At pH 6.0, the midpoints of the unfolding transitions monitored by far-UV-CD and activity measurements (approximately 1.9 and 1.4 M GuHCl, respectively) were shifted to significantly lower [GuHCl] concentrations compared to those at pH 7.4 and 8.5 (Figure 3C). It is also noteworthy that the far-UV-CD and catalytic activity denaturation curves recorded at pH 6.0 are clearly not coincident. The unfolding transition measured using the enzyme's far-UV-CD signal is significantly more shallow than the unfolding transition measured using the enzyme's catalytic activity.

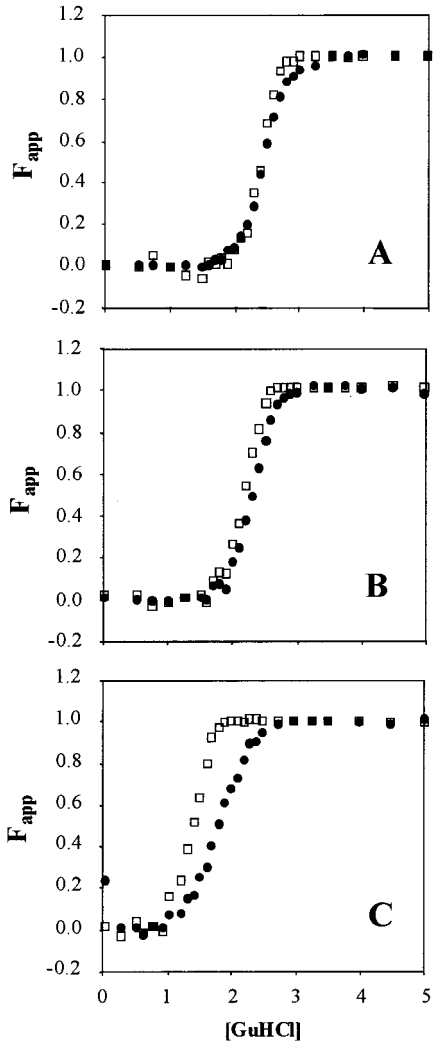

FIGURE 3: Normalized GuHCl-induced equilibrium unfolding curves for wild-type 4-OT at (A) pH 8.5, (B) pH 7.4, and (C) pH 6.0 as monitored by far-UV-CD at 222 nm (closed circles) and by catalytic activity measurements with the substrate 2-HM (open squares). The curves were obtained at 25 °C in 50 mM phosphate buffer at enzyme concentrations of 12, 12, and 10 μM at pHs 6.0, 7.4, and 8.5 (respectively).

GuHCl-Induced Equilibrium Unfolding of Wild-Type 4-OT: Enzyme Concentration Dependence. 4-OT is a multimeric enzyme composed of six identical subunits that are held together entirely by noncovalent interactions; therefore, the apparent stability of the enzyme in our GuHCl-induced equilibrium unfolding studies should depend on protein concentration. Far-UV-CD and catalytic activity denaturation curves recorded at pHs 6.0, 7.4, and 8.5 using protein concentrations ranging from 10 to 150 μM (based on monomer) are shown in Figure 4. Listed in Table 1 are the midpoints of the unfolding transitions that we calculated using eq 5. In these calculations, the concentration of denaturant at which half the protein was folded was determined using the m_g values and the ΔG_{H_2O} values in the table. The midpoints of the unfolding transitions monitored by both far-UV-CD and catalytic activity measurements were shifted to higher GuHCl concentrations with increasing protein concentration at each pH that was studied. Shifts of approximately 0.5 M were apparent over a ~10-fold protein concentration range.

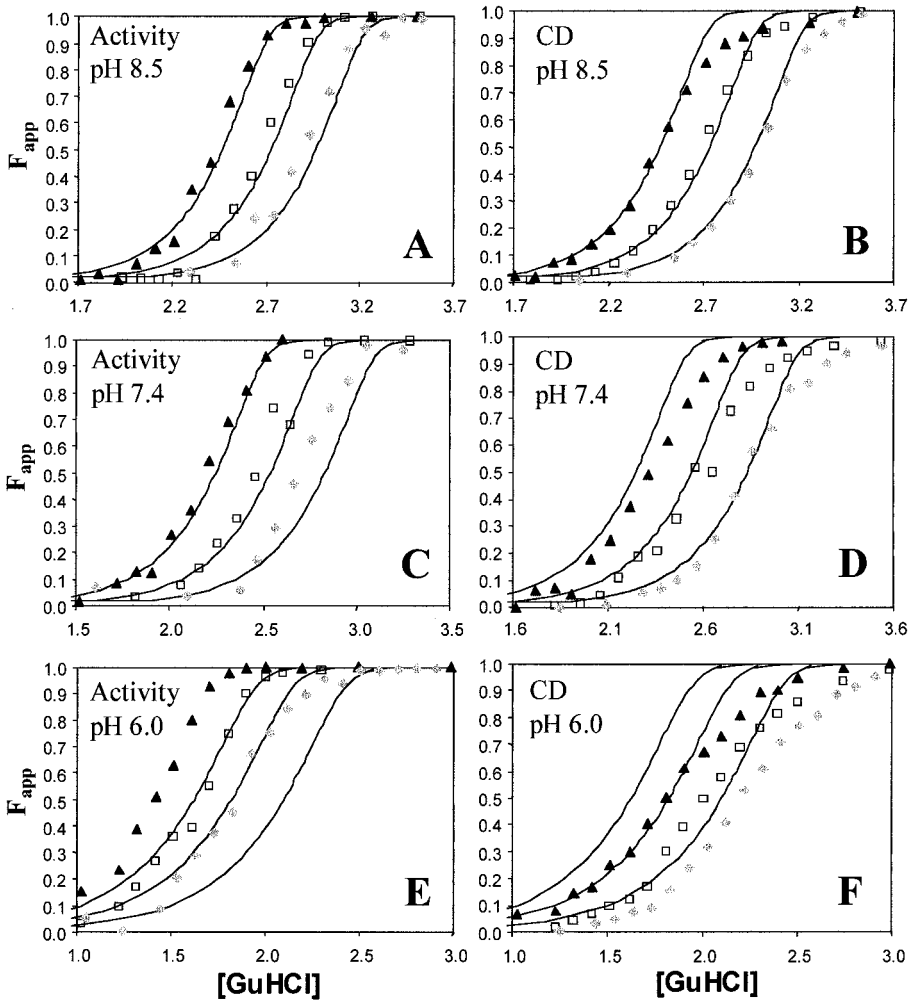

FIGURE 4: pH and the protein concentration dependence of the GuHCl-induced denaturation of 4-OT monitored by far-UV-CD and catalytic activity. The data were obtained at 25 °C in 50 mM phosphate buffer at enzyme concentrations ranging from 10 to 150 μM. The exact enzyme concentrations used at each pH are given in Table 1. In each plot the closed black triangles represent the data recorded at the lowest enzyme concentration, the open squares represent intermediate enzyme concentrations, and the gray diamonds represent the highest enzyme concentration. The solid lines in each plot represent theoretical denaturation curves that were generated using an average ΔG_{H_2O} and m_g values calculated from all the data at each pH and assuming a two-state model model (folded hexamer ↔ unfolded monomer).

Extraction of Thermodynamic Parameters from Equilibrium Data. Thermodynamic parameters, ΔG_{H_2O} and m_g, were obtained from the unfolding curves in Figure 4 using a two-state model for the 4-OT unfolding reaction. The model assumed that the only species populated at equilibrium were the folded hexamer and the unfolded monomer. In our analysis, F_{app} values in the transition region of each denaturation curve in Figure 4 were converted to ΔG_{app} values, and plots of ΔG_{app} vs [GuHCl] were used to calculate ΔG_{H_2O} and m_g values at each pH and protein concentration for each structural probe, as described in Materials and Methods. In all cases, the ΔG_{app} vs [GuHCl] plots were linear as judged by correlation coefficients (>0.94) from linear least-squares analyses.

The ΔG_{H_2O} and m_g values that we obtained from our two-state analysis of the unfolding curves in Figure 4 are summarized in Table 1. If our two-state model is valid then the thermodynamic parameters reported in Table 1 should not vary with the protein concentration or with the structural probe (i.e., far-UV-CD or catalytic activity). Therefore, average ΔG_{H_2O} and m_g values were calculated at each pH using all the data at each pH. The average ΔG_{H_2O} values that we obtained at pHs 6.0, 7.4, and 8.5 were 51.0 ± 2.6, 63.3 ± 3.3, and 68.3 ± 3.1 kcal/mol (respectively). The average m_g values that we obtained at pHs 6.0, 7.4, and 8.5 were −10.1 ± 1.2, −12.8 ± 1.4, and −13.4 ± 0.2 kcal mol^{-1}·M^{-1} (respectively). These average ΔG_{H_2O} and m_g values were then used in eqs 4 and 5 to generate theoretical unfolding curves at each pH and protein concentration for each structural probe (see Figure 4). The theoretical curves that we generated Figure 4 do not exactly coincide with the experimental data. However, it is noteworthy that the theoretical curves we generated at pH 8.5 are most nearly coincident with the experimental data (see Figure 4, panels A and B).

It is possible that the catalytic activity transition is well modeled by a two-state process but that the far-UV-CD transition is not. In this case, the thermodynamic parameters obtained at each pH in Table 1 would vary between the structural probes but would not vary according to protein concentration for each structural probe. This prompted us to generate theoretical curves using the average ΔG_{H_2O} and m_g values that are tabulated in Table 1 at each pH and for each structural probe. The theoretical unfolding curves that we generated using these average values are shown with the

Table 1: Two-State Analysis of the Guanidine-Induced Equilibrium Unfolding of Wild-Type 4-OT at 25 °C

pH	structural probe	denaturation midpoint [GuHCl] (M)[a]	[monomer] (ΔM)[b]	ΔG_{H_2O} (kcal mol^{-1})[c]	m_g (kcal mol^{-1} M^{-1})[c]
6.0	activity	1.4	12	50.9 ± 0.6	−11.4 ± 0.4
		1.7	23	53.3 ± 1.1	−12.4 ± 0.7
		1.9	60	47.0 ± 1.1	−9.2 ± 0.5
	average			50.4 ± 3.2	−11.0 ± 1.6
	CD	1.9	12	49.8 ± 0.8	−8.0 ± 0.4
		2.1	23	54.5 ± 1.2	−10.4 ± 0.6
		2.3	60	50.8 ± 1.4	−9.0 ± 0.6
	average			51.7 ± 2.4	−9.1 ± 1.2
7.4	activity	2.2	12	64.2 ± 1.5	−13.3 ± 0.7
		2.5	42	67.5 ± 2.4	−14.7 ± 1.0
		2.9	149	65.0 ± 2.6	−13.3 ± 0.9
	average			65.0 ± 2.2	−13.8 ± 0.8
	CD	2.4	12	65.7 ± 2.9	−13.1 ± 1.3
		2.7	42	58.2 ± 1.9	−10.3 ± 0.7
		2.9	149	61.1 ± 3.2	−11.7 ± 1.1
	average			61.7 ± 3.8	−11.8 ± 1.4
8.5	activity	2.5	10	73.5 ± 2.1	−15.6 ± 0.9
		2.7	31	70.8 ± 1.6	−14.5 ± 0.6
		2.9	92	70.0 ± 4.0	−14.2 ± 1.4
	average			71.4 ± 1.9	−14.7 ± 0.7
	CD	2.5	10	65.7 ± 1.7	−12.1 ± 0.7
		2.8	31	65.9 ± 2.1	−12.4 ± 0.8
		3.0	92	66.5 ± 1.6	−12.6 ± 0.5
	average			66.0 ± 0.5	−12.4 ± 0.2

[a] Midpoints were calculated using the corresponding ΔG_{H_2O} and m_g values for each denaturation curve. [b] Enzyme concentrations were determined by the Waddell method to within approximately ±10% (*28*). [c] Results were obtained using a two-state model involving native hexamer and unfolded monomer. Values at each protein concentration are reported with standard error from linear least-squares analysis. Average values are reported with a standard deviation.

experimental data in Figure 5. The theoretical unfolding curves that we generated at pH 8.5 are in good agreement with both the catalytic activity and the far-UV-CD transitions that we measured experimentally. This is consistent with our analysis of the pH 8.5 data in Figure 4 from above. At pH 7.4 and pH 6.0, the theoretical unfolding curves that we generated for the activity transitions are in good agreement with the activity transitions that we measured experimentally. However, at pH 7.4 the far-UV-CD unfolding transitions that we observed experimentally are not exactly described by the theoretical curves and the far-UV-CD unfolding transitions that we observed experimentally at pH 6.0 are poorly described by the theoretical curves.

As part of our data analysis we also attempted to fit our data to two other two-state models (one involving native hexamer and unfolded trimer and the other involving native hexamer and unfolded dimer). Considering 4-OT's subunit architecture, both of these alternative models could potentially describe the unfolding of the 4-OT hexamer. The theoretical activity transitions predicted at pH 8.5 and at protein concentrations of 10, 31, and 92 μM using these alternative models are shown with the experimental data in Figure 6. The theoretical curves in Figure 6 were generated using the average ΔG_{H_2O} and m_g values determined at pH 8.5, eq 5, and appropriate versions of eq 4 and eqs 6 and 7, below:

$$K_{app} = \frac{3F_{app}^{3}[P_{tot}]_M^{2}}{1 - F_{app}} \quad (6)$$

$$K_{app} = \frac{2F_{app}^{2}[P_{tot}]_M}{1 - F_{app}} \quad (7)$$

A visual inspection of the data reveals that the theoretical curves obtained using these alternative two-state models clearly do not fit the experimental data (Figure 6).

DISCUSSION

Reversible Denaturation of 4OT. The GuHCl-induced unfolding of 4-OT in 50 mM phosphate buffer is a reversible process at pHs between 6.0 and 8.5 and at protein concentrations between 10 and 150 μM. Enzyme that is denatured in 50 mM phosphate buffer containing 6 M GuHCl rapidly refolds to its native state upon dilution of the GuHCl with 50 mM phosphate buffer. At all the pHs and the protein concentrations used in this study the refolded enzyme was indistinguishable from the wild-type enzyme as judged by far-UV-CD spectroscopy and catalytic activity measurements. GuHCl-induced unfolding curves for 4-OT were also indistinguishable from folding curves of 4-OT that were recorded using these two structural probes.

Apparent Two-State Equilibrium Unfolding of Wild-Type 4-OT at pH 8.5. The GuHCl-induced equilibrium unfolding of 4-OT at pH 8.5 is well modeled by a two-state process that only involves significant populations of folded hexamer and unfolded monomer. Our results indicate that there are no stable intermediate states with substantial helical structure or with measurable amounts of catalytic activity that are significantly populated under equilibrium conditions in 50 mM phosphate buffer at pH 8.5. Several lines of evidence support this conclusion.

One line of evidence supporting our two-state model at pH 8.5 is related to the observation that the unfolding transitions monitored by two structural probes, far-UV-CD spectroscopy and catalytic activity measurements, are nearly

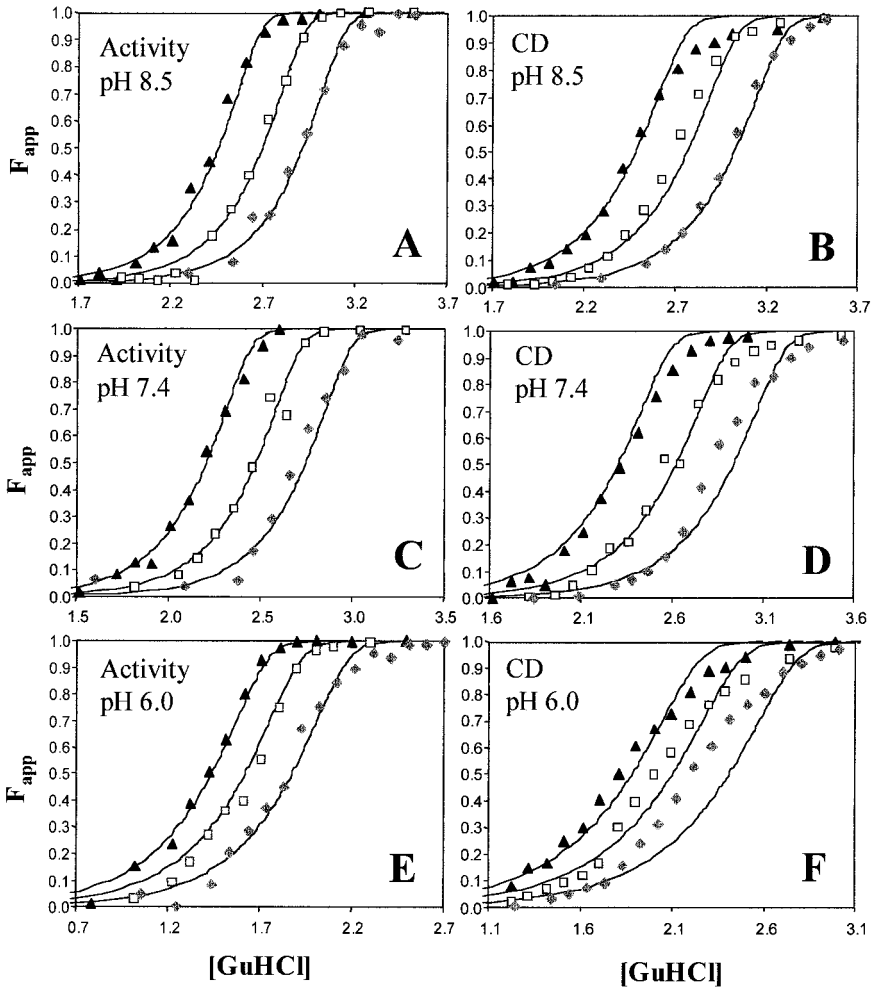

FIGURE 5: pH and the protein concentration dependence of the GuHCl-induced denaturation of 4-OT monitored by far-UV-CD and catalytic activity. All graphs are the same as those shown in Figure 4, with the exception of how the theoretical curves (solid lines) were generated (see text).

identical at pH 8.5 (see Figure 3A). The two structural probes used in our studies provide a sensitive measure of the enzyme's secondary, tertiary, and quaternary structure. The helical content of 4-OT's polypeptide chain in its native state is approximately 25%. Therefore, the presence of such secondary structure is readily determined using far-UV-CD spectroscopy by measuring the enzyme's molar ellipticity at 222 nm. The six active sites in the 4-OT hexamer complex include catalytically important amino acid side chains from at least two different subunits. Therefore, a loss catalytic of activity can be correlated with a loss of 4-OT's tertiary and quaternary structure. The near coincidence of the unfolding transitions monitored by far-UV-CD spectroscopy and catalytic activity measurements at pH 8.5 indicates that tertiary and quaternary structure loss is closely coupled to secondary structure loss in the equilibrium unfolding of 4-OT at this pH.

A second line of evidence supporting our two-state model is related to the protein concentration dependence of the unfolding transitions that we measured at pH 8.5. The protein concentration dependent behavior that we observed at pH 8.5 for the equilibrium unfolding of 4-OT is well described by a two-state model involving only folded hexamer and unfolded monomer. At pH 8.5, the free-energy changes under standard state conditions (i.e., 1 M hexamer) predicted by this two-state model are essentially independent of protein concentration. This suggests that our model appropriately accounts for the enzyme concentration dependence of the equilibrium unfolding of 4-OT in accordance with the Law of Mass Balance (*33*).

Our fitting of the far-UV-CD and catalytic activity data that we obtained at pH 8.5 to a two-state model involving folded hexamer and unfolded monomer yielded an average overall free energy of 68.3 ± 3.2 kcal/mol for 4-OT's unfolding reaction under standard conditions (1 M hexamer). This corresponds to a value of approximately 11 kcal/mol "per monomer unit", which is consistent with several other "per monomer unit" values that have recently been reported in the literature for other homooligomeric proteins including the dimeric Trp repressor protein (which is stabilized by ~10 kcal/mol "per monomer unit") and the tetrameric lactose repressor protein (which is also stabilized by ~10 kcal/mol "per monomer unit") (*9*, *12*). Our two-state analysis of the 4-OT unfolding reaction also yielded an average m_g value of 13.4 ± 1.3 kcal mol^{-1} M^{-1}. The magnitude of m_g values obtained in such a two-state analysis is related to the change in a protein's solvent accessible surface area upon denaturation, and recently, it has been shown that m_g values can be estimated from the size of a protein (*34*). On the basis of an average m_g value per residue of 0.026 ± 0.007 kcal mol^{-1} M^{-1} (from ref *34*) an m_g value of 9.4 ± 2.5 kcal mol^{-1} M^{-1} can be estimated for the 360-amino acid, 4-OT complex. This

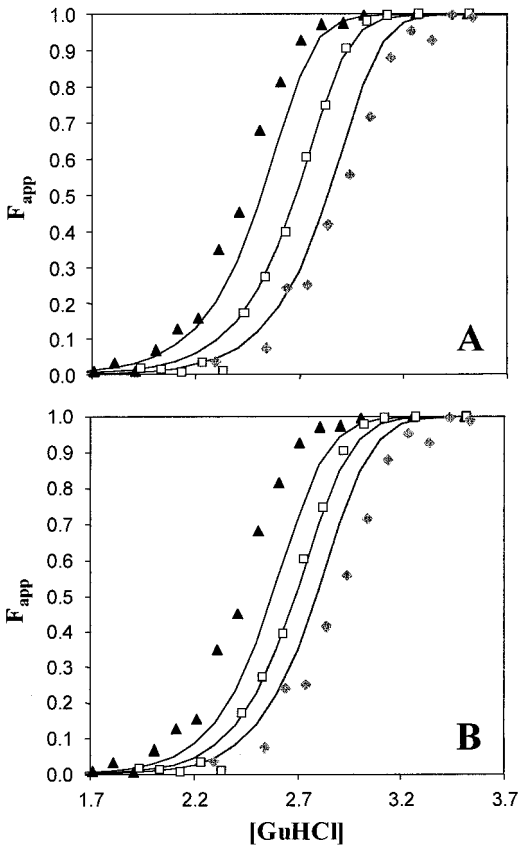

FIGURE 6: Protein concentration dependence of the GuHCl-induced equilibrium unfolding curves for wild-type 4-OT at pH 8.5 as monitored by the enzyme's catalytic activity. The graphs are identical to the graph in Figure 4A with the exception of how the theoretical curves (solid lines) were generated. In panel A, the data was analyzed assuming a two-state equilibrium between a native hexamer and three unfolded dimers. In panel B the data was analyzed assuming a two-state equilibrium between a native hexamer and 2 unfolded trimers.

value is very similar in magnitude to our experimental value, 13.4 ± 1.3 kcal mol^{-1} M^{-1}, which serves to further validate our two-state model for 4-OT's equilibrium unfolding.

In equilibrium unfolding studies of other multimeric proteins it has been observed that the chemically denatured state is not always monomeric (*12*). We attempted to use analytical ultracentrifugation to directly determine the mulitmeric state of a 4-OT sample that was denatured in a 6 M GuHCl solution. Unfortunately, the lack of aromatic residues in 4-OT's primary structure prohibited the use of analytical ultracentrifugation to characterize the oligomeric state of 4-OT in solutions that contain high concentrations of GuHCl. The high absorbance background of such GuHCl containing solutions interferes with the detection of 4-OT molecules in the analytical ultracentrifugation experiment. Therefore, to establish that the end state of 4-OT in our GuHCl denaturation experiments was not an unfolded oligomer we fit our data to two additional two-state models, one that involved folded hexamer and unfolded dimer and one that involved folded hexamer and unfolded trimer. Two-state models involving higher order oligomers in the unfolded state were not considered due the organizational symmetry of 4-OT's subunits (see Figure 1). The two alternative two-state models that we evaluated did not accurately predict the protein concentration dependence of the unfolding transitions we observed (see Figure 6). Clearly, the best fit of our data at pH 8.5 was obtained with a two-state model involving folded hexamer and unfolded monomer (see Figures 4, panels A and B, and 5, panels A and B).

Evidence for Intermediate State(s) in the GuHCl-Induced Equilibrium Unfolding of 4-OT at pH 6.0. The far-UV-CD denaturation midpoints that we recorded for each protein concentration at pH 6.0 and at pH 7.4 were shifted to higher GuHCl concentrations compared to the activity denaturation midpoints that we recorded on the same protein solutions. The shifts were most pronounced at pH 6.0. The noncoincidence of the unfolding transitions measured by far-UV-CD spectroscopy and catalytic activity at pHs 6.0 and 7.4 suggests that intermediate state(s) are populated in the equilibrium unfolding of 4-OT at these pHs. It is also noteworthy that the far-UV-CD unfolding transitions we recorded for each protein concentration at pH 6.0 are more shallow and less cooperative than the unfolding transitions we measured by catalytic activity. The relative position and shape of the far-UV-CD and catalytic activity transitions that we recorded at pH 6.0 suggest the intermediate state(s) populated at this low pH have some elements of helical secondary structure but no significant catalytic activity.

The subunits in the 4-OT complex are organized in a trimer of dimers; therefore, mutlimeric intermediates may exist. The oligomeric state(s) of the intermediates that are populated in the equilibrium unfolding reaction at pH 6.0 cannot be determined from our current data. Work is in progress to construct a fluorescently labeled 4-OT analogue that is amenable to analytical ultracentrifugation experiments in order to better evaluate the oligomeric state of these intermediate states. However, the results reported above do indicate that even if multimeric intermediate states are populated in the equilibrium unfolding of 4-OT they are not catalytically competent.

In conclusion, we have shown that the equilibrium unfolding of the 4-OT homo-hexamer is reversible at pHs between 6.0 and 8.5 and at protein concentrations between 10 and 150 μM. At pH 8.5, the unfolding transitions monitored by far-UV-CD spectroscopy and by catalytic activity are both well described by a two-state model involving folded hexamer and unfolded monomer. At pHs 6.0 and 7.4, only the catalytic activity transition is well described by a two-state model. The far-UV-CD transitions at these lower pHs are significantly more shallow than the catalytic activity transitions. Our results at pHs 6.0 and 7.4 are consistent with the population of intermediate state(s) under equilibrium conditions at these lower pHs; and they suggest that these intermediate state(s) have elements of secondary structure but no measurable catalytic activity.

REFERENCES

1. Schreiber, G., and Fersht, A. R. (1995) *J. Mol Biol. 248*, 478−486.
2. Alber, T., Dao-pin, S., Wilson, K., Wozniak, J. A., Cook, S. P., and Matthews, B. W. (1987) *Nature 330*, 41−46.
3. Koh, J. T., Cornish, V. W., and Schultz, P. G. (1997) *Biochemistry 36*, 11314−11322.
4. Hebert, E. J., Giletto, A.; Sevcik, J., Urbanikova, L., Wilson, K. S., Dauter, Z., and Pace, C. N. (1998) *Biochemistry 37*, 16192−16200.
5. Mirny, L. A., and Shakhnovich, E. I. (1999) *J. Mol. Biol. 291*, 177−196.

6. Chamberlain, A. K., and Marqusee, S. (2000) *Adv. Protein Chem. 53*, 283−323.
7. Schildbach, J. F., Milla, M. E., Jeffrey, P. D., Raumann, B. E., and Sauer, R. T. (1995) *Biochemistry 34*, 1405−1412.
8. Gloss, L. M., and Matthews, C. R. (1997) *Biochemistry 36*, 5612−5623.
9. Gittleman, M. S., and Matthews, C. R. (1990) *Biochemistry 29*, 7011−7020.
10. Dams, T., and Jaenicke, R. (1999) *Biochemistry 38*, 9169−9178.
11. Noland, B. W., Dangott, L. J., and Baldwin, T. O. (1999) *Biochemistry 38*, 16136−16145.
12. Barry, J. K., and Matthews, K. S. (1999) *Biochemistry 38*, 6320−6328.
13. Jaenicke, R. (1987) *Prog. Biophys. Mol. Biol.* 49, 117−237.
14. Chen, L. H., Kenyon, G. L., Curtin, F., Harayama, S., Bembenek, M. E., Hajipour, G., and Whitman, C. P. (1992) *J. Biol. Chem. 267*, 17716−17721.
15. Roper, D. I., Subramanya, H. S., Shingler, V., and Wigley, D. B. (1994) *J. Mol. Biol. 243*, 799−801.
16. Whitman, C. P., Aird, B. A., Gillespie, W. R., and Stolowich, N. J. (1991) *J. Am. Chem. Soc. 113*, 3154−3162.
17. Whitman, C. P., Hajipour, G., Watson, R. J., Johnson, W. H., Bembenek, M. E., and Stolwich, N. J. (1992) *J. Am. Chem. Soc. 114*, 10104−10110.
18. Lian, H., and Whitman, C. P. (1993) *J. Am. Chem. Soc. 115*, 7978−7984.
19. Fitzgerald, M. C., Chernushivech, I., Standing, K. G., Kent, S. B. H., and Whitman, C. P. (1995) *J. Am. Chem. Soc. 117*, 11075−11080.
20. Fitzgerald, M. C., Chernushivech, I., Standing, K. G., Whitman, C. P., and Kent, S. B. H. (1996) *Proc. Natl. Acad. Sci. U.S.A. 93*, 6851−6856.
21. Stivers, J. T., Abeygunawardana, C., Mildvan, A. S., Hajipour, G., and Whitman, C. P. (1996) *Biochemistry 35*, 814−823.
22. Czerwinski, R. M., Johnson, W. H., Jr., Whitman, C. P., Harris, T. K., Abeygunawardana, C., and Mildvan, A. S. (1997) *Biochemistry 36*, 14551−14560.
23. Czerwinski, R. M., Harris, T. K., Johnson, W. H., Jr., Legler, P. M., Stivers, J. T., Mildvan, A. S., and Whitman, C. P. (1999) *Biochemistry 38*, 12358−12366.
24. Nakhle, B. M., Silinski, P., and Fitzgerald, M. C. (2000) *J. Am. Chem. Soc. 122*, 8105−8111.
25. Taylor, A. B., Czerwinski, R. M, Johnson, W. H., Whitman, C. P., and Hackert, M. L. (1998) *Biochemistry 37*, 14692−14700.
26. Murzin, A. (1996) *Curr. Opin. Struct. Biol. 6*, 386-394.
27. Pace, C. N. (1986) *Methods Enzymol. 131*, 266−279.
28. Waddell, W. J. (1956) *J. Lab. Clin. Med. 48*, 311−314.
29. Pace, C. N. (1975) *CRC Crit. Rev. Biochem.* 1−43.
30. Santoro, M. M., and Bolen, D. W. (1992) *Biochemistry 31*, 4901−4907.
31. Marquardt, D. W. (1963) *J Soc. Ind. Appl. Math. 11*, 431−441.
32. Chen, Y., Yang, J. T., and Chau, K. H. (1974) *Biochemistry 13*, 3350−3359.
33. Jaenicke, R., and Lilie, H. (2000) *Adv. Protein Chem. 53*, 329−396.
34. Myers, J. K., Pace, N. C., Scholtz, J. M. (1995) *Protein Sci. 4*, 2138−2148.

BI002752B